PAPER • OPEN ACCESS

ATEP: an advanced transport model for energetic particles

To cite this article: Ph. Lauber *et al* 2024 *Nucl. Fusion* **64** 096010

OPEN ACCESS
IOP Publishing | International Atomic Energy Agency
Nuclear Fusion
Nucl. Fusion **64** (2024) 096010 (9pp)
https://doi.org/10.1088/1741-4326/ad6336

ATEP: an advanced transport model for energetic particles

Ph. Lauber[1,*], M. Falessi[2], G. Meng[1], T. Hayward-Schneider[1], V.-A. Popa[1], F. Zonca[2] and M. Schneider[3]

[1] Max-Planck-Institut für Plasmaphysik, Boltzmannstraße 2, D-85748 Garching, Germany
[2] ENEA, Fusion and Nuclear Safety Department, C. R. Frascati, I-00044 Frascati (Rome), Italy
[3] ITER Organization, Route de Vinon-sur-Verdon, CS90046, 13067 St Paul-lez-Durance, France

E-mail: philipp.lauber@ipp.mpg.de

Received 17 January 2024, revised 11 June 2024
Accepted for publication 15 July 2024
Published 26 July 2024

Abstract

In this paper we report on the implementation and verification of a phase-space resolved energetic particle (EP) transport model. It is based on a first-principle theoretical framework, i.e. the system of non-linear gyrokinetic equations and the related transport equations. Its focus is primarily directed toward understanding the meso-scale character of EPs and its consequences. Compared to the conventional description of thermal radial transport via a one-dimensional radial diffusion equation, the newly developed model is three-dimensional using canonical constants-of-motion (CoM) variables. The model does not assume diffusive processes to be dominant *a priori*, instead the EP fluxes are self-consistently calculated and directly evolved in CoM space. We use the EP-Stability workflow and the HAGIS code to determine the phase space fluxes explicitly either in the limit of constant mode amplitudes or an energy-conserving quasi-linear model. As an application of the model the transport of neutral-beam-generated EPs due to a toroidal Alfvén eigenmode in an ITER plasma is investigated. As there are no sources and collisions taken into account so far (for an extension of the model see the companion paper (Meng *et al* 2024 *Nucl. Fusion* accepted)), the results cannot be considered as an exhaustive study, but rather as a practical demonstration of the conceptual framework on the way to a comprehensive reduced description of burning plasmas.

Keywords: fusion, energetic particles, transport

(Some figures may appear in colour only in the online journal)

1. Introduction

In addition to increasingly realistic non-linear global gyrokinetic simulations [1–6], a hierarchy of theory-based reduced models is highly desirable to complement the predictions concerning the performance of future burning plasmas. Large parameter scans, sensitivity studies, and multi-scale physics describing energetic particle (EP) transport on neoclassical transport time scales require tools that go beyond what is presently feasible with first-principles numerical codes. To this end, in recent years a set of comprehensive transport equations based on non-linear gyrokinetic theory [7–9] have been derived [10–12]. In particular, the special role of EPs has been addressed that not only introduce new classes of resonantly driven instabilities but also interact with micro- and macro-scale plasma perturbations, causing spatio-temporal cross-scale couplings [13, 14]. Within this framework it has been shown that the concept of phase space zonal structures (PSZSs) is a key element to capture the relevant features of EP transport [15]. Evolving the PSZS transport equations, including consistently the EP-generated zonal fields, determines

* Author to whom any correspondence should be addressed.

the new non-linear equilibria that are allowed to deviate substantially from the initial state, requiring a full-F formulation. It can be shown that simpler approaches such as critical gradient models [16], the 'kick' model [17, 18], and quasi-linear resonance broadening models [19, 20] can be recovered in the appropriate limits. The concept of updated non-linear equilibria has also been recently used in connection with ITG turbulence simulations and the formation of internal transport barriers [21].

In this paper we report on the construction, validation, and first application of a reduced EP transport code (named 'ATEP') that aims to capture step by step the comprehensive physics contained in the general equations. Although in its first stages it will not comprise the complete non-linear phenomenology contained in the theoretical framework, its formulation and implementation are designed to eventually capture all relevant non-linear effects in a systematic and transparent way. Whereas this paper neglects sources and collisions, i.e. the formulation is reduced to a 2d transport problem, we demonstrate in a companion paper [22] how the neoclassical part of the problem can be included within the same conceptual framework, leading to a comprehensive 3d EP transport model resolving the time scales needed for the reduced modelling of burning plasmas. It should be emphasised that the omission of sources and collisions in this work limits significantly the physical validity of some results, especially in the cases where simulations on transport time scales $\gtrsim$10 ms are considered. Not only non-resonant collisional relaxation [23] will act on these time scales on the overall EP distribution function, but also the effect of dynamical friction and diffusive scattering on the resonances of the Alfvén mode spectrum [24–27] will influence their non-linear behaviour. Nevertheless, in the view of comparing to previous, collisionless results on Alfvén mode saturation in the quasi-linear regime (e.g. [28]) these results are of interest for verifying the ATEP model hierarchy step by step.

2. Model equations

In its simplest limit without sources, sinks and collisions, the transport equation is formulated as a continuity equation for the EP distribution function F_z in the constants of motion (CoM) phase space (P_ϕ, E, Λ) [12, 29]:

$$\frac{\partial F_z}{\partial t} = -\frac{\partial}{\partial P_\phi}\left(\langle\overline{\frac{\mathrm{d}P_\phi}{\mathrm{d}t}}\rangle F_z\right) - \frac{\partial}{\partial E}\left(\langle\overline{\frac{\mathrm{d}E}{\mathrm{d}t}}\rangle F_z\right). \qquad (1)$$

Here, P_ϕ is the canonical toroidal momentum, E the energy, and $\Lambda = \mu B_0/E$ with μ the adiabatically invariant magnetic momentum that in the absence of collisions remains conserved. Thus, the problem reduces to a 2d equation (P_ϕ, E). $\overline{\langle\rangle}$ indicates orbit and phase (between particles and wave) averaging. Note that notations and definitions deviate slightly from [12]. If the initial F_z is assumed to be a scalar function only of CoM, it will remain independent of any poloidal or toroidal angle since the phase space flow induced by the flow velocity $\mathbf{v}_{P_\phi,E} = (\langle\overline{\frac{\mathrm{d}P_\phi}{\mathrm{d}t}}\rangle, \langle\overline{\frac{\mathrm{d}E}{\mathrm{d}t}}\rangle)$ is also orbit and zonally averaged. For simplicity, we assume here that the flow is incompressible ($\nabla \cdot \mathbf{v}_{P_\phi,E} = 0$). This assumption will be relaxed when the upgraded solver [22] will be also available for the PSZS transport part. Within the constant-amplitude limit of equation (1) we assume that $\mathbf{v}_{P_\phi,E}$ is determined by a (low frequency) fluctuation spectrum with fixed amplitudes, e.g. provided by experimental measurements, comprehensive code results, or a theoretical closure model. That leads to a 2d advection equation with constant advection velocity $\mathbf{v}_{P_\phi,E}$. Evolving equation (1) corresponds to a driven system, where the externally given advection velocities flatten (or also steepen) phase space gradients. If a physical, linearly unstable mode with fixed amplitude, i.e. a prescribed $\delta B/B_0$ (with δB being the radial perturbation of the B-field due to the mode(s) and B_0 the on-axis value of the magnetic field) is chosen to determine $\mathbf{v}_{P_\phi,E}$, phase space (particle) density flows across the phase space volume elements proportionally to the derivatives of F_z. Clearly, phase space density is conserved, but within the constant-amplitude limit the total energy $\mathcal{E}(t) = \int \mathrm{d}v_{P_\phi,E,\Lambda} J_{\mathrm{CoM}} \cdot E \cdot F_{\mathrm{EP}}(t)$ is not conserved. J_{CoM} is the CoM-Jacobian defined below. Monitoring the change in total energy allows one to determine if the perturbations have exhausted the free energy available by flattening F_z, or if the perturbation is starting to pile up energy in an unphysical way. $\mathrm{d}F_z/\mathrm{d}\mathcal{E} = 0$ determines the relaxed state of F_z within this model. For a steady-state solution, one needs to balance this relaxation with sources and sinks. The required neoclassical physics elements have been added to equation (1) and the first promising results, using a bounce averaged collision operator in the same CoM formulation and code framework, are reported in [22].

In order to construct a quasi-linear model, an energy balance between wave amplitude spectrum and phase space flows has to be introduced [29]:

$$\frac{\mathrm{d}}{\mathrm{d}t}\left(\mathcal{E} + \sum_k W_k\right) = -2\sum_k \gamma_{d,k} W_k. \qquad (2)$$

Here, $\sum_k W_k$ is the total wave energy as a superposition of k linear eigenmodes, and $\gamma_{d,k}$ their respective damping rates as inferred from the linear stability solver embedded in the IMAS EP framework (see below). Note that presently only one EP species is considered in equations (1) and (2). Once the change of $\mathcal{E}$ has been calculated for an initial (small) wave spectrum amplitude $\delta B/B_0$ via $\mathbf{v}_{P_\phi,E}(\delta B/B_0)$, the new wave energy can be determined, leading to dynamically changing $\mathbf{v}_{P_\phi,E}(\delta B(t)/B_0)$. This requires to know how $(\langle\overline{\frac{\mathrm{d}P_\phi}{\mathrm{d}t}}\rangle, \langle\overline{\frac{\mathrm{d}E}{\mathrm{d}t}}\rangle)$ behave as a function of the perturbation amplitude. The system conserves phase space density by construction and total energy, if mode damping is ignored or properly accounted for in the energy balance. If the wave spectrum is not allowed to change its shape, i.e. if non-linear mode structure modifications are ignored, the model is similar to the HAGIS model [30], at least in the limit when only one perturbation is considered. For a multi-mode system, the relative amplitude change between different modes is ignored so far, however, this is in line with a quasi-linear model where mode saturation amplitude and effective linear growth rates are directly

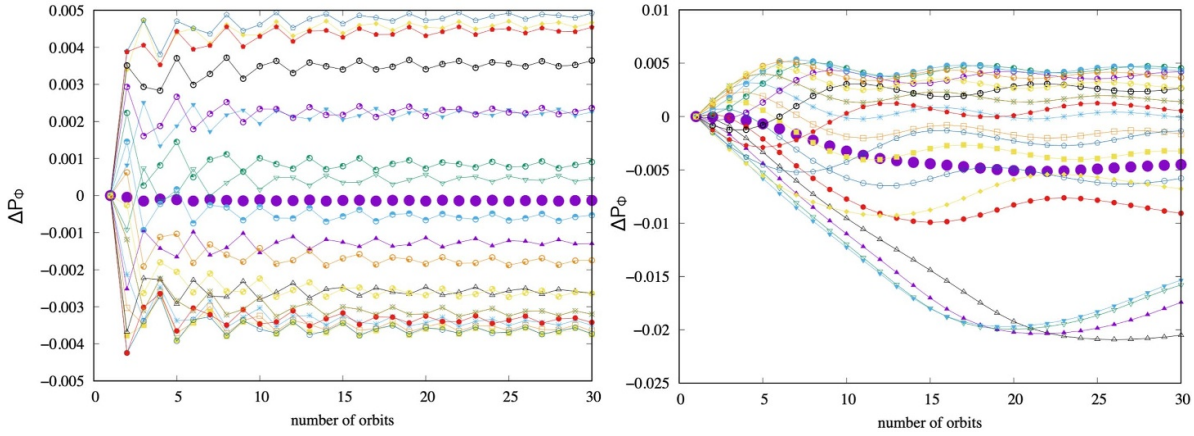

Figure 1. Ensemble of particles with different toroidal phases (different colours) with respect to an $n = 13$ TAE at fixed amplitude ($\delta B/B_0 = 5 \cdot 10^{-4}$) representing one point in CoM space: on the left ($P_\phi = -0.015$, $E = 200\,\mathrm{keV}$, $\Lambda = 0.0017$) the passing particles are non-resonant, the average $\Delta P_\phi = P_{\phi,t} - P_{\phi,\mathrm{start}}$ is vanishing. On the right ($P_\phi = -0.015$, $E = 200\,\mathrm{keV}$, $\Lambda = 0.84$) the barely passing particles are resonant. For not too large perturbations, ΔP_ϕ initially grows proportional to the number of transits, at later times the particles have been 'transported' and remain at their final position. For typical parameters $\delta B/B_0 \lesssim 5 \cdot 10^{-3}$ averaging over five orbits leads to accurate and reasonably fast results for $\langle \overline{\Delta P_\phi/\Delta t} \rangle$. The phase averaged P_ϕ is plotted as well (full dots). Note that P_ϕ here is normalised to $Ze\psi$ with ψ the poloidal magnetic flux at the last closed flux surface.

correlated. It should be remarked, that whereas equation (1) deals explicitly with fluxes in CoM space, the equation can also be cast as an advection-diffusion equation in the quasi-linear limit [31]. By determining the autocorrelation time τ_{ac} (note that the resonance conditions for all CoM positions and the damping/growth rates for the perturbations are known) the diffusion coefficients can be readily calculated: $D_{P_\phi,P_\phi} = \langle \overline{\frac{\mathrm{d}P_\phi}{\mathrm{d}t}} \rangle^2 \cdot \tau_{\mathrm{ac}}$, and similarly for the energy and mixed diffusion tensor elements. As the particle database contains also all mappings from P_ϕ to various orbit averaged radial coordinates (R, poloidal flux, toroidal flux), a radial diffusion coefficient in $\mathrm{m}^2\,\mathrm{s}^{-1}$ units can be constructed for the use in standard transport codes.

3. Implementation

The newly written ATEP code is technically closely interlinked with the well-established IMAS (Integrated Modelling and Analysis Suite) framework and its data structures [32]. It profits in design and modularity from the recently established EP-stability workflow (WF) used in this paper to calculate the linear mode spectrum [33]. The interfaces between the different codes employ IMAS data structures, meaning that all operations needed to set up the ingredients for the PSZS evolution equations are in principle replaceable by equivalent codes or models.

Using the linear gyrokinetic mode information (radial structure, frequency, damping/growth rate) as given by the LIGKA code [34] embedded in the EP-stability WF, the well-established HAGIS code [30] is employed to calculate the response $\langle \overline{\mathrm{d}P_\phi/\mathrm{d}t} \rangle$ and $\langle \overline{\mathrm{d}E/\mathrm{d}t} \rangle$ for a set of pre-selected sample markers for different perturbation amplitudes. First, a set of markers covering the whole CoM space, including co- and counter-passing particles is generated by a code wrapper called 'Orbit-Finder' with a prescribed grid CoM resolution ($128 \times 40 \times 40$ in this paper). The grids are refined close to the trapped passing boundary, and all orbit properties, such as topological status, transit time, averaged precession drift, and average radial position are determined by following all particles for one orbit in the equilibrium configuration. Note that this information can be used to determine the local Jacobian $J_{\mathrm{CoM}} = \frac{(2\pi)^2 E}{ZemB_0} \Sigma_{\sigma=\pm1} \tau_{t,b}$ where Ze is the charge of the ion, m its mass, σ the sign of the particle's parallel velocity with respect to the background magnetic field B_0 and $\tau_{t,b}$ the transit/bounce time of the particle. Note that in the following co- ($\sigma = 1$) and counter-passing ($\sigma = -1$) grids are treated separately, as these can regions overlap in P_ϕ, E, Λ space. In order to ensure smooth transitions across topological boundaries, trapped and other non-standard-orbit regions are included in both co- and counter-passing grids. Selected quantities such as $\tau_{t,b}$ or J_{CoM} are divided by 2 in order to avoid double counting.

After setting up the grid and determining basic orbit properties, a perturbation (or set of perturbations) is added to the unperturbed magnetic field at a fixed amplitude $\delta B/B_0$, and the markers are followed for $N = 5 - 10$ orbits (see figure 1). In addition, each marker in CoM space is replaced by $\sim$10 identical markers that are started with a different phase in the toroidal angle $2\pi/n_{\mathrm{tor}}$, where n_{tor} is the toroidal mode number of the perturbation. For a multi-mode case, the lowest toroidal mode number is typically used, or a random phase seed can be chosen. This procedure is a very effective zonal and orbit average procedure, since now $\langle \overline{\mathrm{d}P_\phi/\mathrm{d}t} \rangle$ for each marker can be recorded, and averaged over N orbit transits and all toroidal phases. The initial jump for some of the non-resonant particles

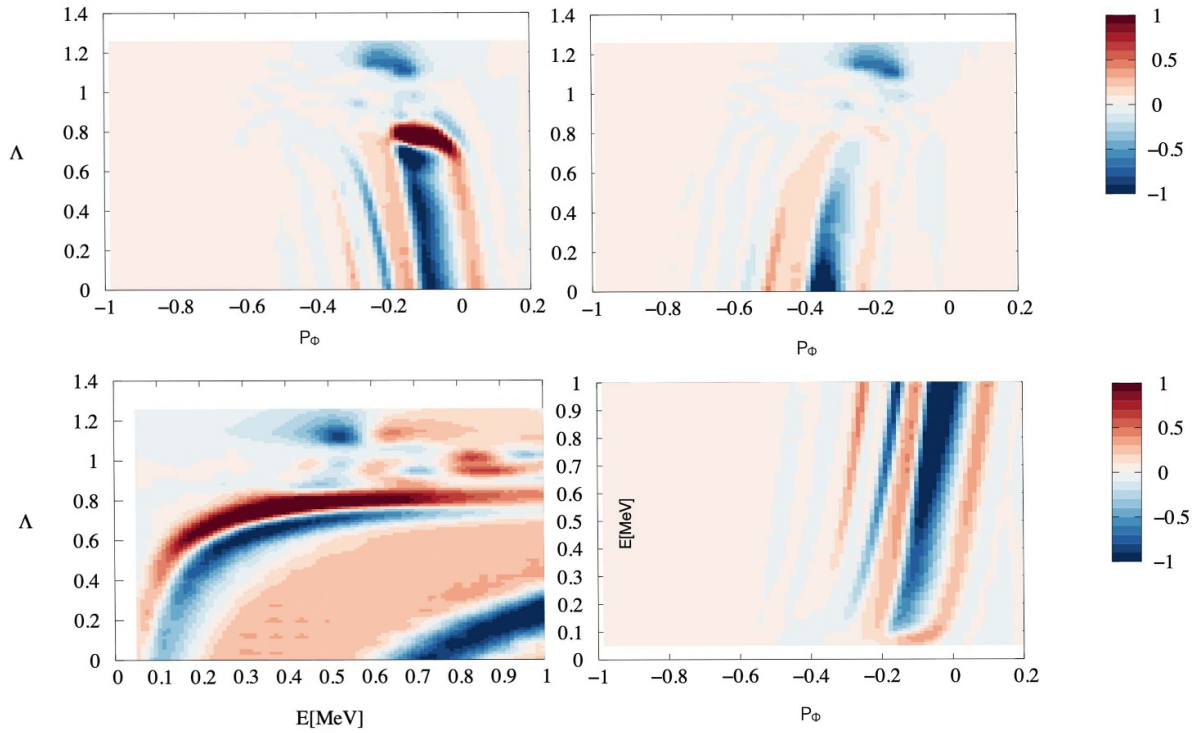

Figure 2. $\langle \overline{\mathrm{d}P_\phi/\mathrm{d}t} \rangle$ for a single $n = 13$ TAE with $\delta B/B = 5 \cdot 10^{-6}$ as a function of the CoM space for different slices: left top: co-passing and trapped particles, right top: counter-passing and trapped particles for $E = 500$ keV. Bottom left: E–Λ plane with $\Lambda = \mu B_0/E$ for $P_\phi = -0.2$; bottom right: P_ϕ–E plane for $\Lambda = 0.12$ (deeply passing particles). Blue/red colours refer to outward/inward transport (negative/positive P_ϕ direction). Note that P_ϕ is normalised to $Ze\psi$ with ψ the poloidal magnetic flux at the last closed flux surface.

in figure 1 is caused by the fact that these particles 'see' on their first orbit a new effective magnetic field due to the perturbation, depending on their starting position. Resonant particles instead, experience a gradual displacement due to their nearly constant phase with respect to the perturbation.

Note that this averaging can be replaced by determining the phase space island width and the related transport time across the island for each phase space position. For the case shown in figure 1 both methods lead to very similar values for $\langle \overline{\mathrm{d}P_\phi/\mathrm{d}t} \rangle$. A more comprehensive comparison between the two methods will be reported in future work. $\langle \overline{\mathrm{d}E/\mathrm{d}t} \rangle$ is calculated similarly. As expected, a linear relation between $\langle \overline{\mathrm{d}P_\phi/\mathrm{d}t} \rangle$ and $\langle \overline{\mathrm{d}E/\mathrm{d}t} \rangle$ is found due to the conservation properties of the wave-particle system.

It should be noted that the dynamics of strongly unstable perturbations with ballistic transport (i.e. particles remain only a fraction of their individual orbits in the perturbations' potential) is not properly captured by this procedure as for these CoM positions the transport coefficient may be underestimated. However, as we aim to construct a transport model for long time scales, this phenomenology is ignored for now, although the theoretical framework has been developed beyond this limit, as exemplified for chirping fishbones in [35]. In order to quantify (and to improve, if necessary) the simplifications related to this procedure, a connection to detailed analyses of transport scaling laws (diffusive/convective) for both Alfvénic gap and EP modes is in progress [36, 37]. Clearly, 2d loss patterns cannot be captured by the model, as it relies on an orbit-averaging procedure. However, the new non-linear equilibria can be used as input to particle tracking codes that are able to deliver detailed loss information. The IMAS integrated 'FINDER' tool used here as a HAGIS-wrapper for calculating the orbit averages is also employed to determine the orbit-averaged collision coefficients, using the collisional version of the HAGIS code [22, 38].

The calculated transport coefficients can be projected onto the final 3d CoM grid used in the ATEP code (typically 64–96 grid points per P_ϕ, E, Λ and mode amplitude, but higher resolutions are possible). A multi-level spline interpolation algorithm [39] is used in order to set up $\mathbf{v}_{P_\phi,E}(\delta B/B_0)$ from the somewhat scattered (loss boundaries, refinement at trapped passing boundary) HAGIS data on the regular CoM grid. The results are shown in figure 2, where co- and counter-passing CoM grids have been separated [40]. However the trapped grid is kept for both cases in order to ensure smooth splining across topological boundaries. Main and higher-order resonances can be seen, showing the phase-space dependent transport properties of a resonant toroidal Alfvén eigenmode (TAE) perturbation. Any projection to a lower dimensional transport coefficient would neglect energy and pitch angle dependencies that turn out to be especially important for the calculation of zonal currents.

In this paper, we use the METIS-generated ITER pre-fusion scenario simulation #100015/1, and TAE mode with toroidal mode numbers $n_{\mathrm{tor}} = 13$ (see figure 3). For this simulation, three different neutral beam generated EP distribution functions (hydrogen) as calculated by the NEMO/SPOT WF [41] are available: one with both beams on-axis, one

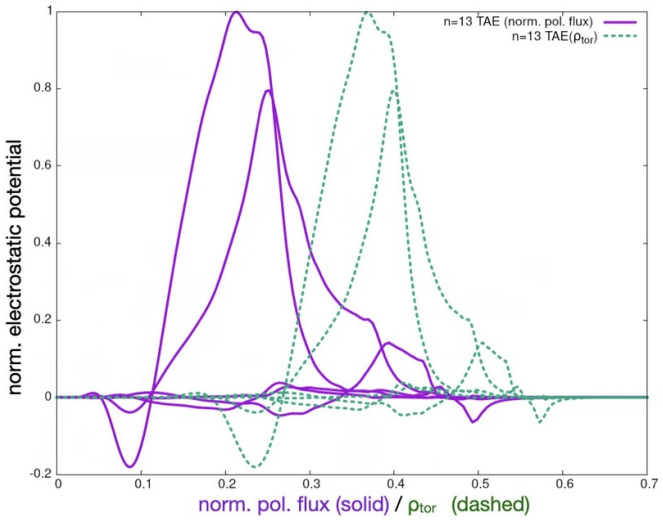

Figure 3. Electrostatic potential of the $n = 13$ TAE with $f = 75.5$ kHz as calculated with LIGKA using the EP-Stability workflow. In order to compare to figures 6 and 7, it is plotted as function of the normalised poloidal flux (solid) and the $\varrho_{\rm tor}$(dashed).

with both beams off-axis, and a mixed on-off-axis case. The NEMO/SPOT results are stored as a set of markers in the IDS *distribution*, containing the complete set of spatial and velocity coordinates, together with the canonical CoM coordinates and the marker weights. Clearly, any other code giving the same information can be readily used as input.

The marker data is imported into the ATEP code similarly to the $\mathbf{v}_{P_\phi,E}(\delta B/B_0)$ data. Depending on the marker resolution, binning, smoothing and splining of this original F_{EP} is required. Obviously, there is some arbitrariness in this process. Here, we first bin the markers into the regular CoM grid described above, and then construct a 2d spline in each of the sub-spaces (P_ϕ, E) , (P_ϕ, Λ) and (E, Λ). Individual smoothing can be applied for each of the sub-grids. Then, a 3d spline is constructed and the derivatives with respect to P_ϕ and E are determined. The result can be seen in figure 4.

After these preparation steps equation (1) can be evolved in time. Being a 'simple' advection (diffusion) problem, standard methods in the literature can be used. So far we employ an explicit 2nd order Lax–Wendroff-scheme with automatic time step adoption (Courant-limit check) and a Matlab based implicit Crank–Nicolson solver for testing. A final choice of the solver, including parallelisation and performance optimisation will be made at a later time.

The preparation of the input for ATEP requires moderate computational effort: depending on the model, the runtime for EP-stability WF is a couple of seconds to a few minutes [33]. Preparing the orbit- and zonally-averaged data typically requires 10 min on 32 cores (ITER SDCC cluster). Although this step is already parallelised it can be further optimised and accelerated in the future. Reading, binning, and splining take about 30 s, depending on the CoM grid resolution. Finally, the transport equation evolution is quite fast, however the Courant criterion for the explicit solver may require small time steps. The implicit solver [22] resolves this problem, but still needs parallelisation for larger CoM grids. The time-advanced $F_{\rm EP}$ on the CoM grid is remapped into the marker-space by updating the individual weights of markers belonging to a certain CoM position according to the change of phase space density at that position. It becomes obvious, that the markers themselves are not transported, just their weights are evolved according to the PSZS fluxes. Then, standard averages and moments can be taken to determine density, current, and pressure in physical units. This information, or the EP diffusion coefficients discussed above, can be passed to a comprehensive transport code. In summary, all ingredients for solving the PSZS transport equation and its interfaces to other transport codes have been established. For details on the collisional part, please refer to the companion paper [22].

4. First results

As in figure 2 we use the even $n = 13$ TAE at various fixed amplitudes to evolve the system, i.e. equation (1). At each time step, the energy of $F_{\rm EP}$ is determined via integrating over CoM space and normalising to the initial energy E_0: $\mathcal{E}(t) = \int {\rm d}v_{P_\phi,E,\Lambda} J_{\rm CoM} \cdot E \cdot F_{\rm EP}(t)/E_0$. Density conservation is enforced, as in this case no outflux from the CoM grid is allowed. As discussed above, we assume $\nabla \cdot \mathbf{v}_{P_\phi,E} = 0$. Losses and transport to thermal energies (the energy boundary was set to 50 keV) are ignored so far. As shown in figure 5, the total energy stored in F_{EP} decreases due to the PSZS fluxes. That means that the perturbation is able to extract energy from the gradient of $F_{\rm EP}$, as it is expected for an unstable TAE. Note, that for perturbations that are not consistently chosen as unstable eigenmodes of the system, the total energy can also increase, meaning that the perturbations increase $\mathcal{E}(t)$. In this example, $\mathcal{E}(t)$ decreases linearly in the first phase, its linear decay rate being proportional to the applied $\delta B/B_0$. Plotting the same data $1 - \mathcal{E}(t)$ on a log t scale shows how the same amount of energy is extracted on very different time scales for different $\delta B/B_0$. As the perturbation amplitude is held fixed, at some point, the free energy is exhausted, and the total energy reaches a minimum. As $\delta B/B_0$ remains fixed in the constant-amplitude limit and damping is ignored, the phase space density is further evolved. This requires energy, and thus the total energy starts to increase again. Including sources and collisions [22] balancing the EP transport, will lead to consistent saturation levels. We can use the minimum in $\mathcal{E}(t)$ to define a maximally relaxed state. In figure 6 such a relaxed zonal state $\delta F_{\rm EP} = F_{\rm EP}(t) - F_{\rm EP}(t = 0)[10^{16}\,{\rm m}^{-3}]$ is plotted in two different projections. One can see that—as expected—the transport is mainly radially outwards. Also, high-energy phase space density is reduced and lower-energy regions are more strongly populated. This illustrates how different CoM regions of the beam $F_{\rm EP}$ drive and damp the perturbation, i.e. how EP energy is channelled on average via Landau damping to low-energy regions (α-channelling [42]). Projecting $F_{\rm EP}$ from the CoM grid back to real space and taking moments allows us to

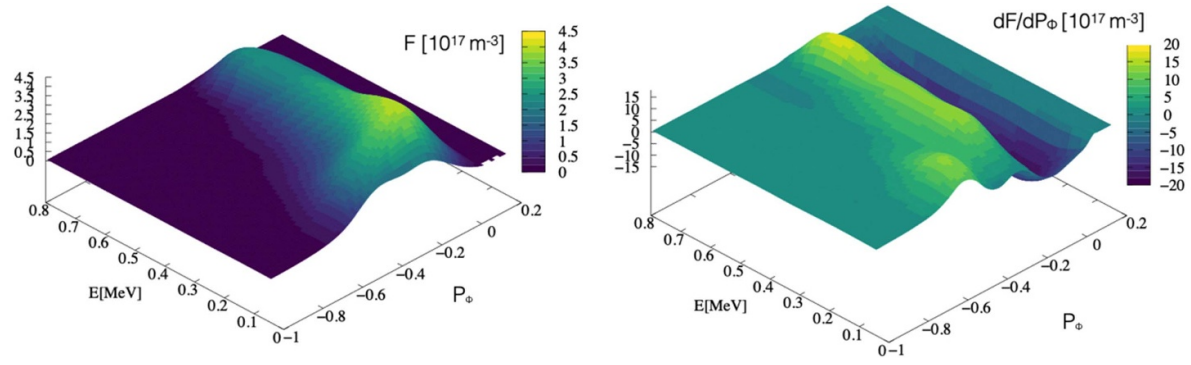

Figure 4. Distribution function of energetic hydrogen particles, #100015/1, in ITER's off-off-axis beam configuration. The original marker data as calculated by the NEMO/SPOT package was binned, smoothed, splined and projected onto the regular CoM grid of the ATEP code (slice with $\Lambda = 0.5$) .

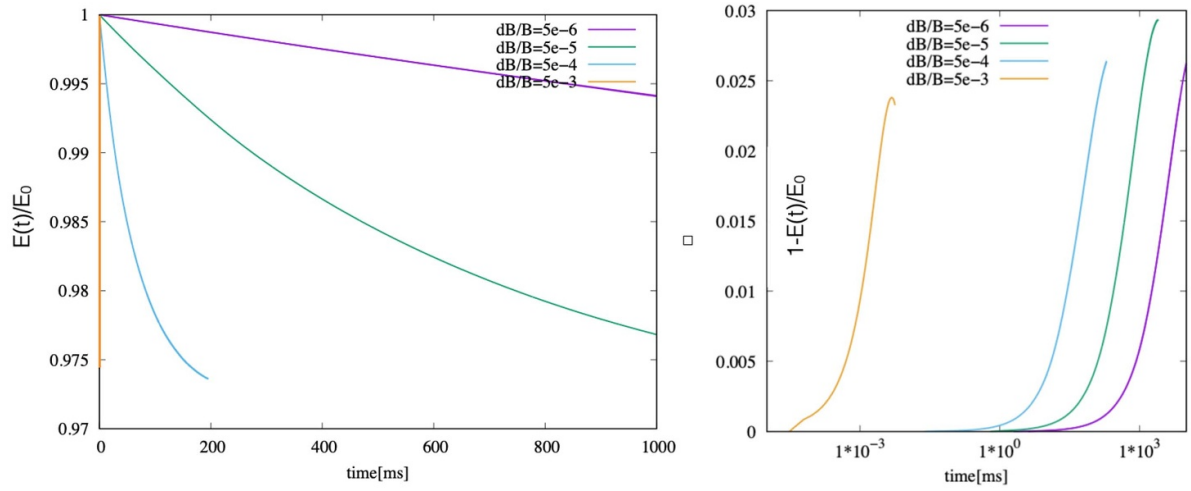

Figure 5. Linear (left) and logarithmic (right) time evolution of the normalised total energy $\int \mathrm{d}v_{P_\phi,E,\Lambda} E \cdot F_{\mathrm{EP}}(t)/E_0$ using the constant-amplitude limit for #100015/1, in ITER's off-off-axis beam configuration for a fixed TAE with different amplitudes.

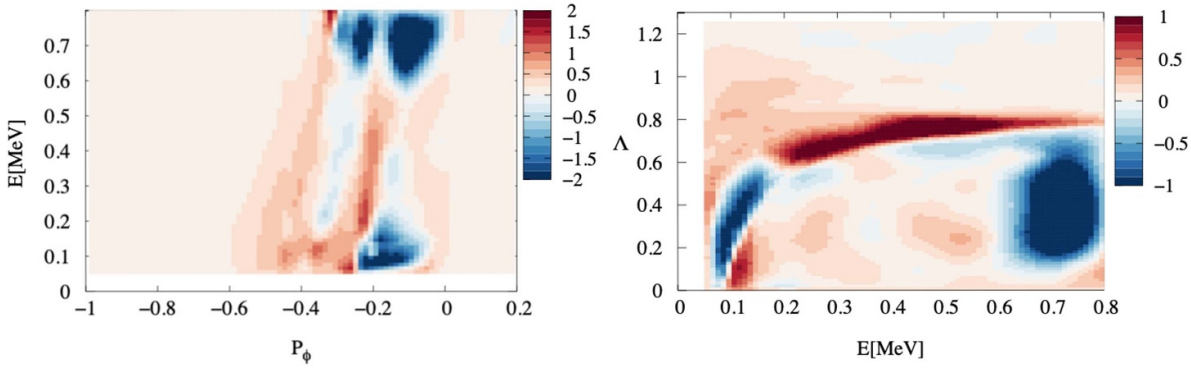

Figure 6. Left: the PSZS state $\delta F_{\mathrm{EP}} = F_{\mathrm{EP}}(t = 700\,\mathrm{ms}) - F_{\mathrm{EP}}(t = 0)[10^{16}\,\mathrm{m}^{-3}]$ for #100015/1 (off-off-axis beam configuration) in the constant-amplitude limit with $\delta B(t)/B_0) = 10^{-5}$ in (P_ϕ, E) plane, integrated over Λ ; right: $\delta F_{EP}[10^{16}\,\mathrm{m}^{-3}]$ in (E, Λ) plane integrated over P_ϕ. Here, F_{EP} as shown in figure 4 was used.

determine the zonal density and the zonal current that represent the radial transport of EP density and current, as plotted in figure 7. One can see how F_{EP} is relaxed, i.e. the gradients flattened and EP density and current are transported radially outwards, as theoretically expected. Clearly, this information can be used to construct a new non-linear equilibrium, and by using a sensible iteration scheme, the ATEP code can be cast into a reduced full-F EP transport model.

As described above, this model can be improved by evolving the wave energy consistently with the change of $\mathcal{E}(t)$. To this end, a set of $\mathbf{v}_{P_\phi,E}(\delta B/B_0)$ for $\delta B/B_0 = [10^{-6}, 10^{-5}, 10^{-4}, 10^{-3}]$ is prepared as described above. A

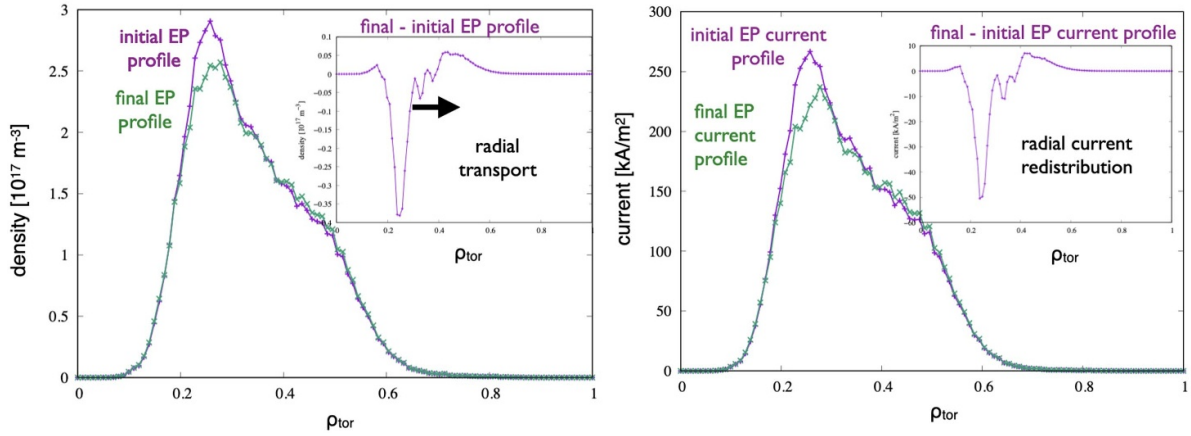

Figure 7. Left: radial projection ($\varrho_{\rm tor}$) of the distribution function of energetic hydrogen particles, #100015/1, in ITER's off-off-axis beam configuration, initial (as given by NEMO/SPOT) and final state after evolving the PSZS transport equation for 700 ms (1000 time steps) in the constant-amplitude limit with $\delta B(t)/B_0) = 10^{-5}$; right: the initial and final EP-current for the same case. The inlets in both plots show the difference of the final and the initial state.

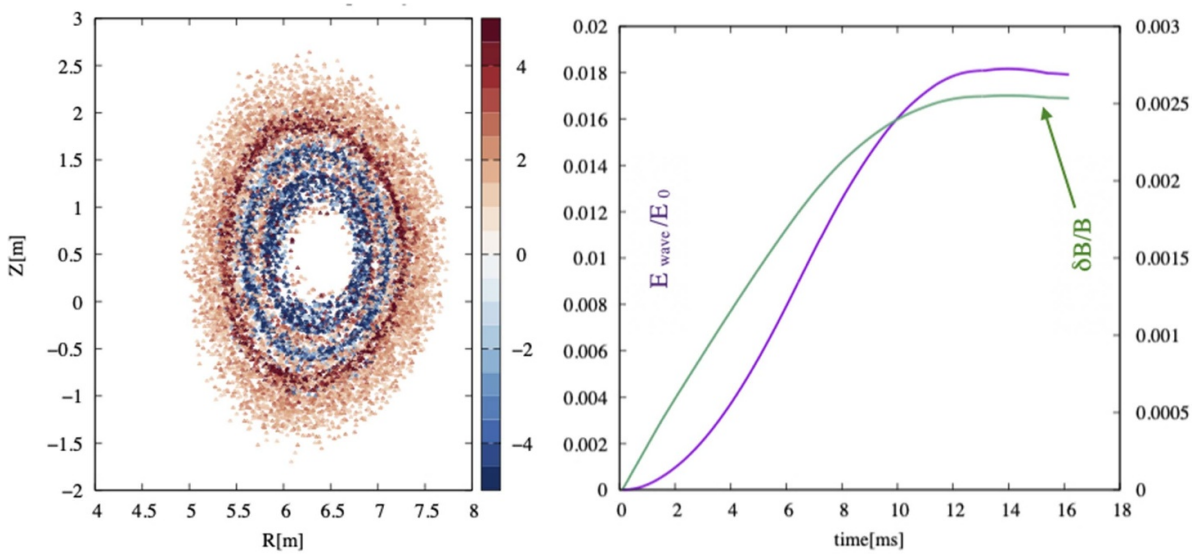

Figure 8. Left: for the same case as shown in figure 6: mapping back the PSZS to marker space shows that the transport equation indeed introduces a zonal density perturbation to F_{EP}, here represented as the change of marker weights (%) (colour bar). For this plot only the most resonant particles with $E > 500$ keV and $\Lambda < 0.3$ were chosen. Right: the normalised wave energy $E_{\rm wave}(t)/E_0$ and $\delta B(t)/B_0$ are allowed to evolve dynamically according to the energy balance equation (2). After an initial growth phase, saturation and a starting decay is observed.

4D spline (3 CoM coordinates and $\delta B/B_0$) is constructed. Whereas the amplitude dependence is simple for a single mode (essentially the orbit width of the EPs determine the volume of CoM space that is affected by the spatially fixed perturbation), resonance overlap criteria for multi-mode cases can be accurately taken into account by this procedure. As discussed in the previous section, here 'multi-mode' refers to a mode spectrum with fixed relative amplitudes where a global energy balance can be applied. If individual module evolution needs to be described or linearly stable spectra are destabilised non-linearly, an individual energy balance needs to be constructed in order to calculate the non-linear growth rates and related particle fluxes. This extension is presently under development. Using the fact that the wave energy is $\sim(\delta B/B_0)^2$, one can map the change of $\mathcal{E}$ for a small initial perturbation to $(\delta B(t)/B_0)^2$, leading to a stronger initial growth of the perturbation until a saturated $B_{\rm max}/B_0$ is reached (see figure 8). Since no background damping is included so far, the mode decays only very slowly due to the growing imbalance of beam damping and drive. Including realistic background damping rates will allow us to reach reasonable saturation amplitudes, in line with the non-linear wave-particle interaction model implemented in HAGIS.

5. Conclusions and outlook

After the first encouraging results reported here, a further thorough validation effort will be carried out, profiting from ongoing work within the Eurofusion Enabling Research Project

'ATEP'. To that end, comparisons with other reduced models will be carried out, e.g. with an ongoing extension of the DAEPS code [12, 43] that uses explicit analytical expressions for calculating the phase space fluxes. Also, a 1d reduced model based on the beam-plasma bump-on-tail paradigm that is designed to go beyond the quasi-linear approximation and thus forecast possible EP transport transitions such as avalanching [36] will be used to determine the limits of the ATEP model. As mentioned above, its formulation allows one to carry out detailed analysis of transport scaling laws (diffusive/non-diffusive) using e.g. Lagrangian coherent structures (LCS) [36, 37, 44]. Further verification and validation are being carried out using comprehensive numerical codes in the appropriate limits (HYMAGYC, (X)HMGC, ORB5, HAGIS/LIGKA; for a recent benchmark of these codes refer to [4, 45]). To that end, the implementation of PSZS diagnostics in the various codes [46, 47] provides a natural connection point for detailed comparisons. In addition, the Hamiltonian mapping method, as pioneered within the HMGC code, gives further valuable insight into trapping/detrapping processes in single and multi mode systems [46, 48, 49] building on the same LCS methods developed for the 1d beam-plasma model. After validation, the ATEP model will be extended to include non-linear interactions via direct and in-direct (i.e. mediated by ZS) coupling mechanisms as described in [10, 12–15]. Several time-dependent scenarios from present-day and future experiments (particularly AUG, JT-60SA, TCV, DTT, JET, ITER) have already been collected and ported into IMAS for validation and uncertainty quantification [33]. Motivated by the particular needs of the ATEP project for validation cases, dedicated experiments at AUG have been designed and carried out. Building on previously developed scenarios that maximise the ratio of EP vs. background pressure [50], strongly EP-driven mode activity and EP transport in plasmas with different isotope mixes have been observed and are presently analysed.

Acknowledgments

This work has been carried out within the framework of the EUROfusion Consortium, funded by the European Union via the Euratom Research and Training Programme (Grant Agreement No. 101052200—EUROfusion). Views and opinions expressed are however those of the author(s) only and do not necessarily reflect those of the European Union or the European Commission. Neither the European Union nor the European Commission can be held responsible for them. ITER is the Nuclear Facility INB No. 174. The views and opinions expressed herein do not necessarily reflect those of the ITER Organisation.

ORCID iDs

M. Falessi https://orcid.org/0000-0002-2105-226X
G. Meng https://orcid.org/0000-0002-0969-733X
T. Hayward-Schneider https://orcid.org/0000-0003-0588-5090
V.-A. Popa https://orcid.org/0000-0002-3099-4857
F. Zonca https://orcid.org/0000-0002-9270-4704

References

[1] Mishchenko A. *et al* 2023 *Plasma Phys. Control. Fusion* **65** 064001
[2] Hayward-Schneider T., Lauber P., Bottino A. and Mishchenko A. 2022 *Nucl. Fusion* **62** 112007
[3] Biancalani A. *et al* 2023 *J. Plasma Phys.* **89** 905890602
[4] Vlad G. *et al* 2021 *Nucl. Fusion* **61** 116026
[5] Di Siena A. *et al* (the ASDEX Upgrade Team and the EUROfusion MST1 Team) 2022 *Nucl. Fusion* **62** 106025
[6] Brochard G. *et al* 2022 *Nucl. Fusion* **62** 036021
[7] Frieman E. and Chen L. 1982 *Phys. Fluids* **25** 502–8
[8] Sugama H. 2000 *Phys. Plasmas* **7** 466–80
[9] Brizard A.J. and Hahm T.S. 2007 *Rev. Mod. Phys.* **79** 421 (48
[10] Falessi M.V. and Zonca F. 2019 *Phys. Plasmas* **26** 022305
[11] Zonca F., Chen L., Falessi M.V. and Qiu Z. 2021 *J. Phys.: Conf. Ser.* **1785** 012005
[12] Falessi M.V., Chen L., Qiu Z. and Zonca F. 2023 *New J. Phys.* **25** 123035
[13] Chen L. and Zonca F. 2016 *Rev. Mod. Phys.* **88** 015008
[14] Zonca F., Chen L., Briguglio S., Fogaccia G., Milovanov A.V., Qiu Z., Vlad G. and Wang X. 2014 *Plasma Phys. Control. Fusion* **57** 014024
[15] Zonca F., Chen L., Briguglio S., Fogaccia G., Vlad G. and Wang X. 2015 *New J. Phys.* **17** 013052
[16] Waltz R. and Bass E. 2014 *Nucl. Fusion* **54** 104006
[17] Podestà M., Gorelenkova M. and White R.B. 2014 *Plasma Phys. Control. Fusion* **56** 055003
[18] Podesta M., Gorelenkova M., Gorelenkov N.N. and White R.B. 2017 *Plasma Phys. Control. Fusion* **59** 095008
[19] Gorelenkov N., Duarte V., Podesta M. and Berk H. 2018 *Nucl. Fusion* **58** 082016
[20] Meng G., Gorelenkov N., Duarte V., Berk H., White R. and Wang X. 2018 *Nucl. Fusion* **58** 082017
[21] Wang S., Wang Z. and Wu T. 2024 *Phys. Rev. Lett.* **132** 065106
[22] Meng G., Lauber P., Lu Z., Bergmann A. and Schneider M. 2024 *Nucl. Fusion* **64** 096009
[23] Gaffey J.D. 1976 *J. Plasma Phys.* **16** 149–69
[24] Berk H., Breizman B., Fitzpatrick J. and Wong H. 1995 *Nucl. Fusion* **35** 1661
[25] Berk H., Breizman B. and Pekker M. 1996 *Phys. Rev. Lett.* **76** 1256–9
[26] Lilley M., Breizman B. and Sharapov S. 2009 *Phys. Rev. Lett.* **102** 195003
[27] Duarte V., Berk H., Gorelenkov N., Heidbrink W., Kramer G., Nazikian R., Pace D., Podesta M., Tobias B. and Zeeland M.A. 2017 *Nucl. Fusion* **57** 054001
[28] Schneller M., Lauber P. and Briguglio S. 2016 *Plasma Phys. Control. Fusion* **58** 014019
[29] Kaufman A.N. 1972 *Phys. Fluids* **15** 1063–9
[30] Pinches S.D. *et al* 1998 *Comput. Phys. Commun.* **111** 133–49
[31] Chen L. 1999 *J. Geophys. Res.* **104** 2421–7
[32] Imbeaux F. *et al* 2015 *Nucl. Fusion* **55** 123006
[33] Popa V.-A., Lauber P., Hayward-Schneider T., Schneider M., Hoenen O. and Pinches S. 2023 *Nucl. Fusion* **63** 126008
[34] Lauber P., Günter S., Könies A. and Pinches S.D. 2007 *J. Comput. Phys.* **226** 447–65
[35] Zonca F. *et al* 2023 *Proc. 29th IAEA FEC (London, UK, 2023)* (available at: https://conferences.iaea.org/event/316/contributions/28449/)
[36] Carlevaro N., Montani G., Falessi M. and Lauber P. 2022 *48th EPS Conf. on Plasma Physics* (*Maastricht*, 27 *June–1 July 2022*) p P5a.113 (available at: https://info.fusion.ciemat.es/OCS/EPS2022PAP/pdf/P5a.113.pdf)

[37] Milovanov A.V., Rasmussen J.J. and Dif-Pradalier G. 2021 *Phys. Rev.* E **103** 052218
[38] Bergmann A., Peeters A.G. and Pinches S.D. 2001 *Phys. Plasmas* **8** 5192–8
[39] Lee S., Wolberg G. and Shin S.Y. 1997 *J. IEEE Trans. Vis. Comput. Graph.* **3** 228–44
[40] Bierwage A., Fitzgerald M., Lauber P., Salewski M., Kazakov Y. and Štancar Ž. 2022 *Comput. Phys. Commun.* **275** 108305
[41] Schneider M., Lerche E., Eester D.V., Hoenen O., Jonsson T., Mitterauer V., Pinches S., Polevoi A., Poli E. and Reich M. 2021 *Nucl. Fusion* **61** 126058
[42] Fisch N. and Rax J.-M. 1992 *Phys. Rev. Lett.* **69** 612–5
[43] Li Y., Falessi M.V., Lauber P., Li Y., Qiu Z., Wei G. and Zonca F. 2023 *Plasma Phys. Control. Fusion* **65** 084001
[44] Carlevaro N., Falessi M.V., Montani G. and Zonca F. 2015 *J. Plasma Phys.* **81** 495810515
[45] Vlad G. *et al* 2023 *Proc. 29th IAEA FEC (London, UK, 2023)* (available at: https://conferences.iaea.org/event/316/contributions/28121/)
[46] Briguglio S., Wang X., Zonca F., Vlad G., Fogaccia G., Di Troia C. and Fusco V. 2014 *Phys. Plasmas* **21** 112301
[47] Bottino A. *et al* 2022 *J. Phys.: Conf. Ser.* **2397** 012019
[48] Wang X., Briguglio S., Di Troia C., Falessi M., Fogaccia G., Fusco V., Vlad G. and Zonca F. 2022 *Phys. Plasmas* **29** 032512
[49] Wang X., Briguglio S., Bottino A., Falessi M., Hayward-Schneider T., Lauber P., Mishchenko A., Villard L. and Zonca F. 2023 *Plasma Phys. Control. Fusion* **65** 074001
[50] Lauber P. *et al* 2018 *EX/1-1 Proc. 27th IAEA FEC (Gujarat, India, 22–27 October 2018)* (available at: https://conferences.iaea.org/event/151/contributions/6094/)